HERA Memorandum Number 1, January 23, 2015
Confusion limited imaging on PSA64

C.L. Carilli[1,2]

ccarilli@aoc.nrao.edu

ABSTRACT

I present results from imaging with PSA64 in an imaging configuration at $18'$ resolution. The results represent a classic example of confusion limited imaging.

1. Basic parameters and initial processing

PAPER in South Africa was in a imaging configuration with 64 antennae in the Summer of 2011. The antennas were distribued roughly randomly, in a circular region with a maximum baseline of 300m. I have self-calibrated and imaged data from July 4, 2011. The results are interesting in that they are a classic demonstration of confusion limited imaging.

Observations were made over the standard PAPER band, but I have limited my analysis to 140MHz to 180MHz. A single linear polarization was observe, although I am not sure which one.

Initital processing in AIPY (by Pober) involved basic flagging, initial phase and amplitude calibration, and phase-to-zenith for 10min blocks. These data have gone through standard AIPY compression, with a resulting record length for a visibility of 42.95sec (a nice round number). The data were then converted to FITS format and transfered to AIPS.

Within AIPS, the FITS header was initially incorrect. I had to change the Stokes parameter to correspond to a single polarization. I also had to change the coordinate equinox to year 2000, since the initial header thought it was 2230. The data were then sorted to Time-Baseline order, as needed for some of the subsequent processing.

[1]National Radio Astronomy Observatory, P. O. Box 0, Socorro, NM 87801

[2]Cavendish laboratory, Cambridge University, UK

Figure 1a shows the UV-plane distribution for a single channel for a 10min observation of the zenith. Figure 1b shows an amplitude – baseline UV plot. I clipped all UV points stronger than 2000Jy.

2. Self-calibration and imaging

Each 10min block of data was imaged and deconvolved using IMAGR in aips with Briggs weighting of the visibilities with R=0, and a uv-minimum of 15lambda. The UVmin was used to avoid residual interference and/or cross talk. Cubes of 8 channels from 140 to 180MHz were generated, and the channels CLEANed to a residual surface brightness of typically 5Jy beam^{-1}.

The UV data were then self-calibrated using the CLEAN model from the imaging, with a 2min averaging time. Figure 2 shows some of the typical solutions from self-calibration. The gain corrections were typically $< 20\%$. The phase solutions showed overall trends on the scale $< 10^o$, but sometimes offsets of up to 50^o. Such corrections could be due to missing structure in the input model, although, since the resulting images were in fact improved after self-calibration, it seems more likely that these were real corrections.

Flagging on gain solutions can be a powerful tool for removing bad data. I found that 6 antennas had very poor self-calibration solutions, meaning amplitude corrections a factor 2 or more worse (typically much worse), than most antennas. These antennas were flagged and self-calibration redone. For reference, the AIPS antenna numbers for these were: 3, 33, 38, 41, 54, 56.

The synthesized beam has a FWHM $\sim 18'$, with a peak sidelobe of -0.22. Figure 3 shows a profile image of the synthesized beam. Removing the uvmin in the imaging step did not alter the peak sidelobe substantially (-0.21).

After imaging in blocks of 10min with 8 channels from 140MHz to 180MHz, the cubes were 'squashed' to a single channel (straight averaging), then different time blocks were shifted to fixed field center using HGEOM, and summed. No correction was made for the primary beam.

Figure 4 shows an image for data in which the Galactic plane was visible. This image is the sum of 4 x 10min blocks, duly averaged and shifted. The Galactic plane shows the standard broad sidelobes due to missing short spacings.

Figure 5 shows an image of 50min of data when the Galactic plane is either very low in the primary beam, or has set. The peak on the image is 65 Jy beam^{-1}, corresponding to

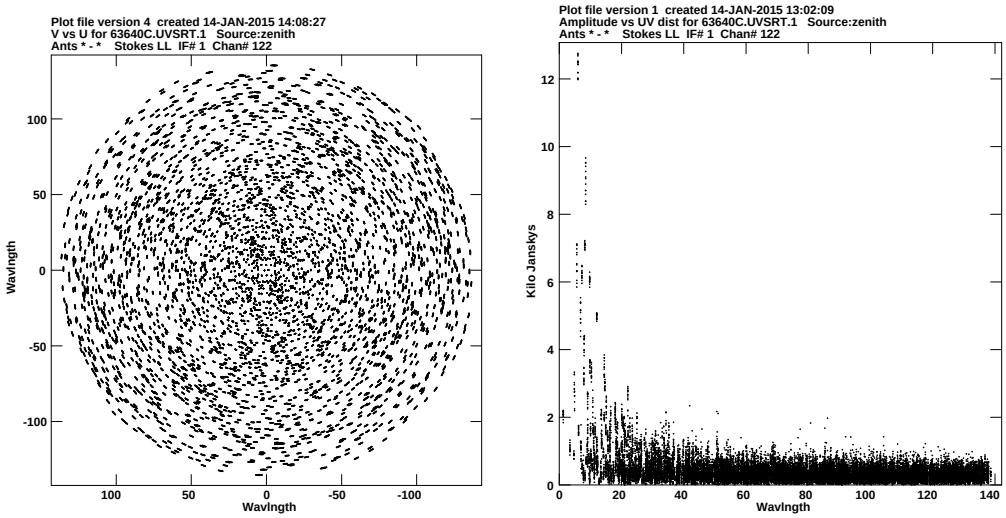

Fig. 1.— Left: The UV coverage of a single channel of PSA64 for 10min of data at 160MHz for PSA64. Right: A UV plot of amplitudes vs. baseline length for a high Galactic latitude field.

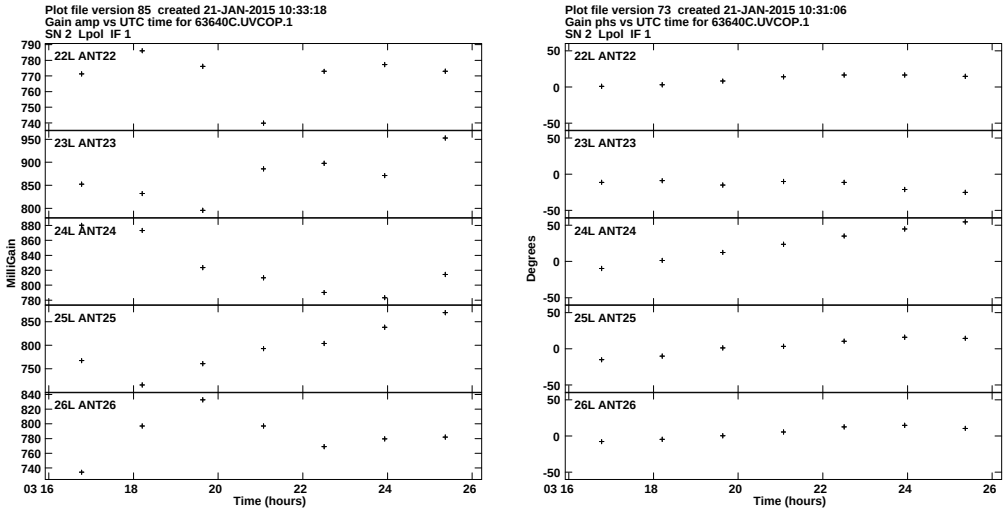

Fig. 2.— Left: Typical antenna-based amplitude self-calibration solutions for PSA64 for 10min of data, with 2 min averaging of solutions. Right: Typical phase self-calibration solutions for PSA64.

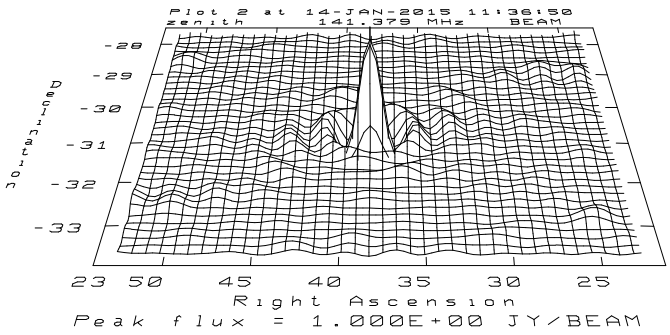

Fig. 3.— The PSA64 PSF in profile for robust=0 imaging, for 10min of data at 160MHz.

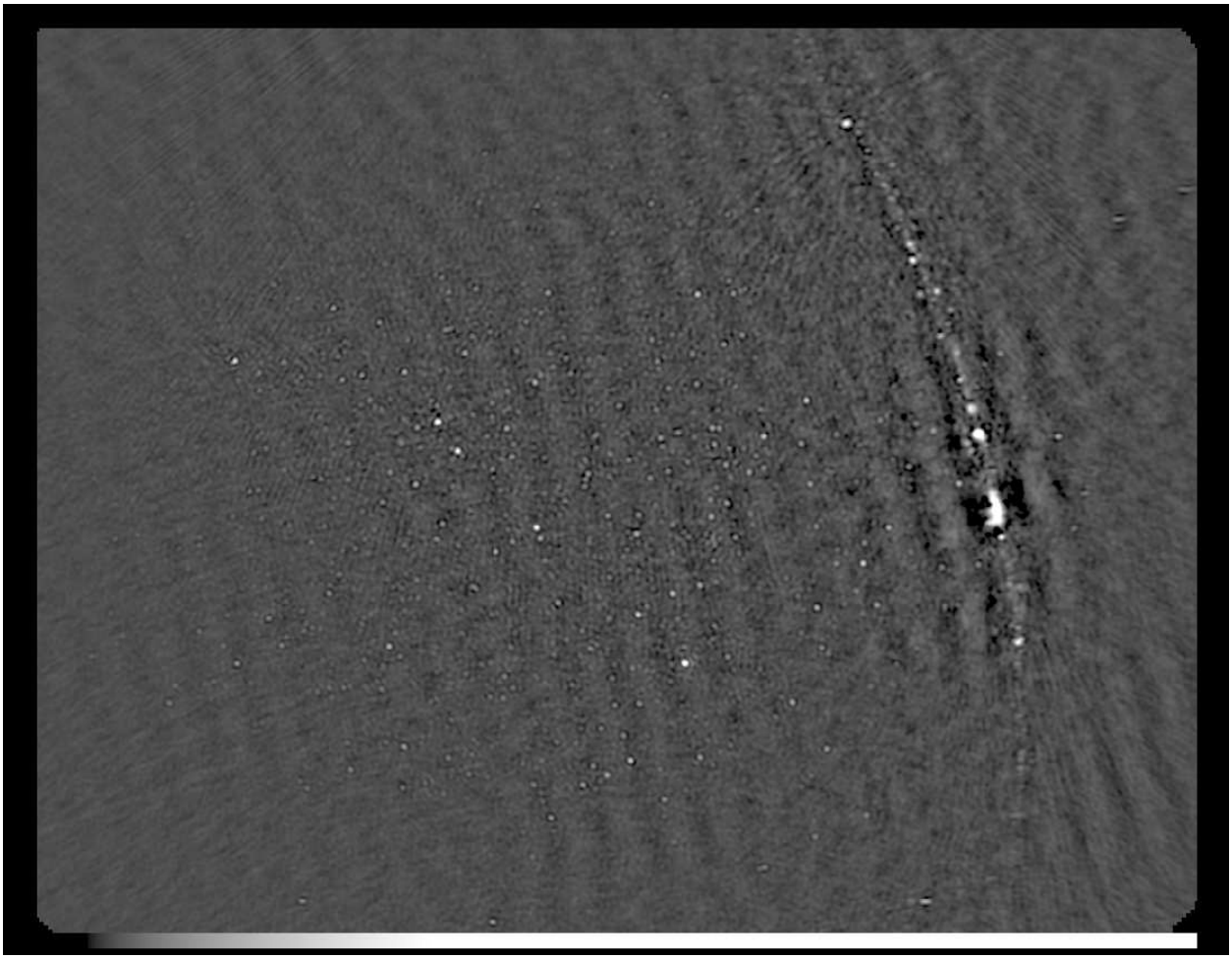

Fig. 4.— A 40min PSA image when the Galactic plane is up, averaged over 140 to 180MHz. The PSF has a FWHM of 18′.

the source J2214-170. Sidelobes can still be seen from some sources well outside the primary beam, such as Cygnus A, which appears in a few time blocks on the northern edge of the field. The rms of surface brightness fluctuations at the edges of the field is about 90mJy beam^{-1}, while that in the field center is about 1.5Jy beam^{-1}.

3. Confusion limited imaging

The most curious aspect of Figure 5, as compared to higher frequency, higher resolution interferometric imaging with eg. the VLA, is that the apparent 'noise' in the center of the field is much higher than at the edges. This behaviour is prior to primary beam correction, ie. just the Fourier Transform of the Visibilities. Typical VLA images at higher frequency and resolution will show a flat noise characteristic across the field, prior to primary beam correction. This noise characteristic is clearly due to confusion – the field is 'full of stars'.

Figure 6 shows a profile image of the field center. This image shows very little space within the field center that is absent of sources plus their inner sidelobes.

Another way of looking at this is Figure 7. Figure 7 shows that the character of the noise is radically different in the inner and outer parts of the field. The inner part of the field is essentially filled with sources. It is hard to identify positions that are not associated with a source, or its immediate sidelobes. The outer part of the field, where the attenuation of the primary beam greatly limits celestial sources, shows noise characteristics probably still dominated by far-out sidelobes of the brightest sources (large-scale structures washing over the image), plus thermal noise fluctuations.

An interesting trend in the center of the field is that the sidelobes for stronger sources are no stronger than for weaker sources. This result is due to the imaging process. Each field was decovolved only in short time and frequency blocks. Hence, only the brighter sources get CLEANed. The PSF sidelobes of the fainter sources only appear when the blocks are summed to the final image.

The flux scale is at best approximate, since I have averaged in both frequency and time, making no correction for primary beam or source spectra. Still, as a rough estimate of whether the flux scale and astrometry is anywhere close to correct, I compare two sources from the Helmbodt et al. (2008) catalog with the results in Figure 5.

The first Helmboldt source is J221425.7-170141.2. They quote a flux density at 160MHz of 80Jy. I obtain a position of J221403.277-170105.92, within a few arcmin of the Helmboldt position, and a flux density of 65Jy. This source is about 25^o from the field center, or

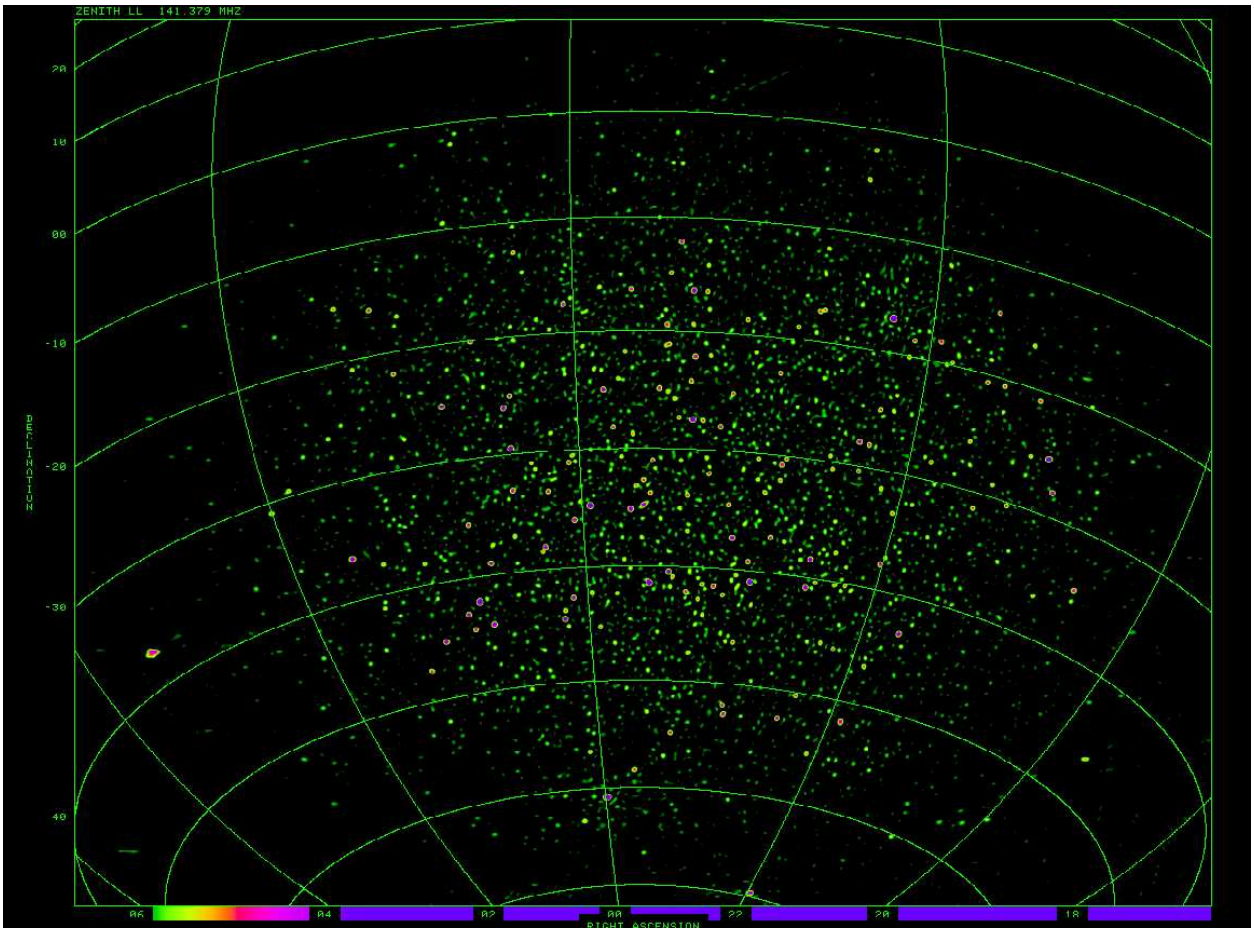

Fig. 5.— A PSA64 image from 50min of data averaged from 140MHz to 180MHz of a high Galactic latitude field. The PSF has a FWHM of 18′.

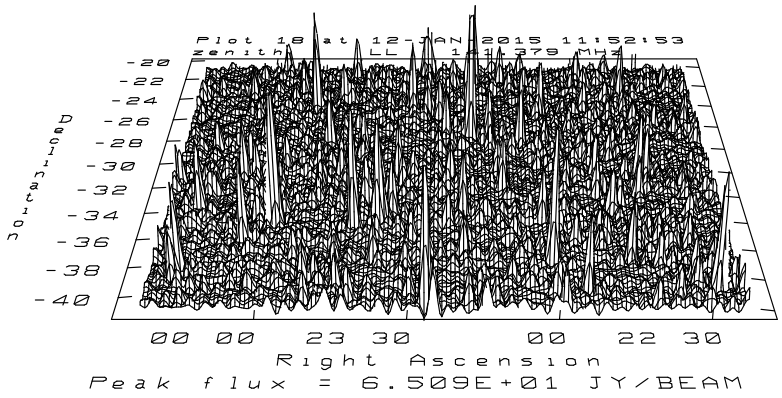

Fig. 6.— A profile image of the field center from Fgiure 5.

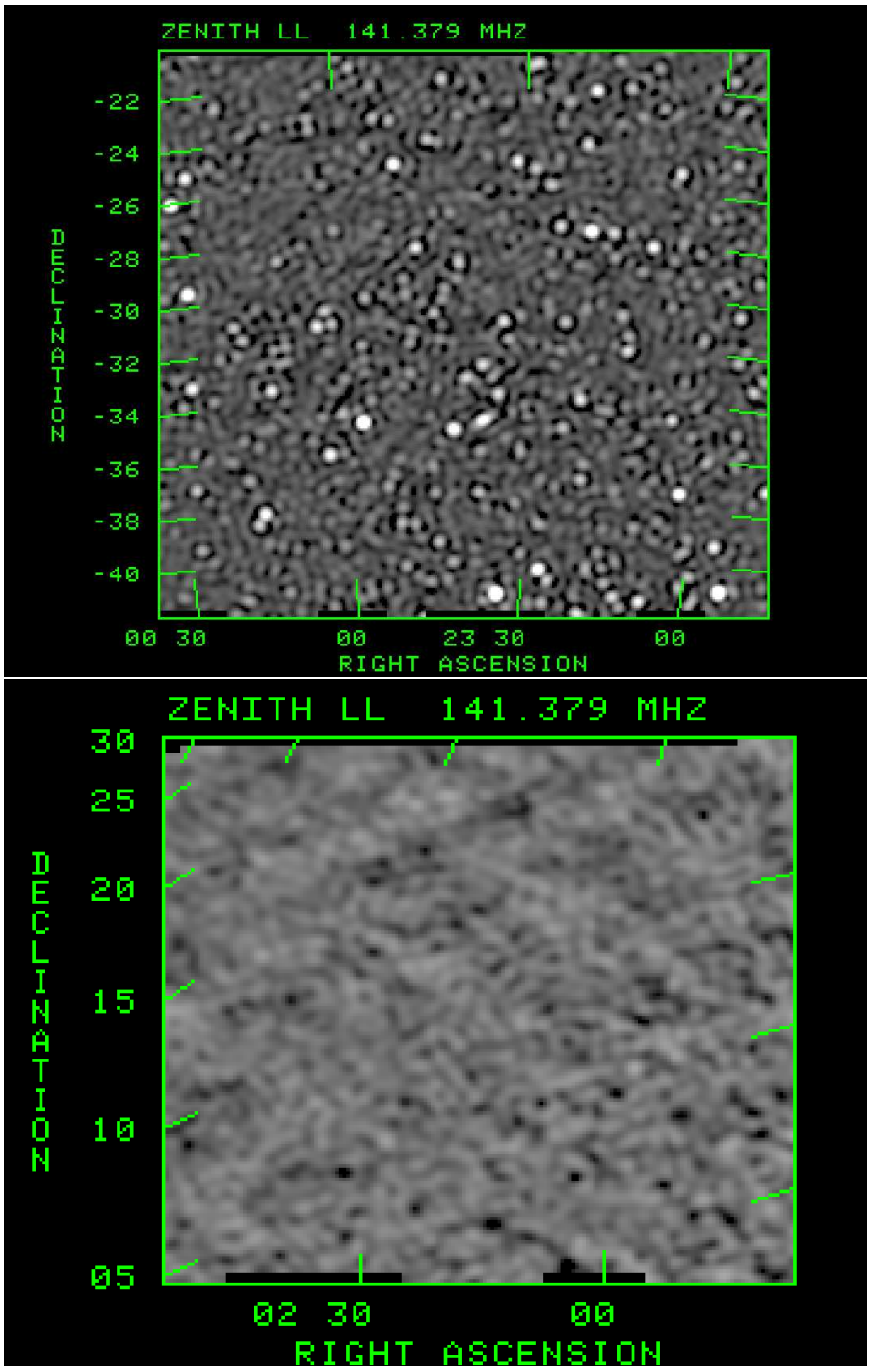

Fig. 7.— Top: An image of the field center. Bottom: an image of the outer part of the field. Note how even the faint peaks in the top figure show signatures of the PSF.

just beyond the half power point of the Primary Beam (although this also depends on the different time blocks summed for the final image). Hence, my flux scale may be a bit high, perhaps by $\sim 40\%$.

A second source from Helmboldt is J000322.1-172711.1, for which the extrapolated flux density at 160MHz is 9.4Jy. I obtain a position of J000314.66-173043.75, again within a few arcmin, and a flux density of 10.7Jy. This source is more about 15^o from the field center, again suggesting perhaps my flux scale is high by about 40%.

4. Confusion noise and the Primary Beam

First I consider the P(D) of the pixel surface brightness distribution. Such an analysis is standard for confusion limited imaging, such as in the recent JVLA deep fields at 8GHz by Condon et al. 2012 (ApJ, 758, 23).

Figure 8a shows the normalized P(D) distribution for the center of the field in Figure 5, and for the edge of the field. Again, the rms of fluctuations at the edge of the field is about 90mJy beam^{-1}, while that in the field center is about 1.5Jy beam^{-1}. For comparison, assuming 50min integration for PSA64, a bandwidth of 40MHz, an effective element area of 9 m^2, and $T_{sys} \sim 560$K (Pober et al. 2014, 782, 66), the expected thermal noise is 11 mJy beam^{-1}. The implication is that, even in the outer parts of the field, the noise is dominated by far-out sidelobes of distant sources. While such noise could also be considered 'confusion', since it relates to cosmic sources, it will not follow the shape of the primary beam, since it is due to sources well away from the position of interest. Hence, I will lump this into a spatially flat noise distribution, as would also be expected for thermal noise in a non-primary beam corrected image.

The confusion noise shows both a broader distribution in P(D), and a clearly non-Gaussian tail to large values – the classic signature of confusion noise in interferometric imaging (Condon et al. 2014). The negative part of the distribution is dictated by non-CLEANed, near-in sidelobes of the confusing sources. The tail to large positive surface brightnesses are the brighter sources themselves. I return to this point below.

The drop off in the confusion noise in Fig. 5 presents a visual image of the primary beam. This would be strictly true in the case when there is no thermal noise, and the PSF had no far-out sidelobes. In our case, there is both thermal noise, and far-out sidelobes due to both point sources and diffuse emission. Hence, the following analysis gives at best a gross estimate of the primary beam and behaviour of the noise.

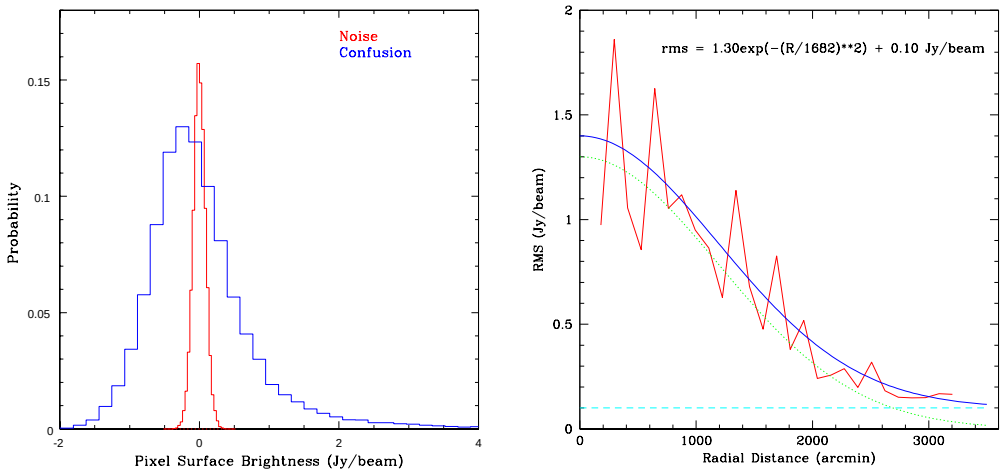

Fig. 8.— Left: The P(D) distribution of the pixel surface brightness distribution. The red curve is the 'noise' field, in the outer part of the primary beam, and the blue curve is at the confusion dominated field center. Right: The rms of the surface brightness fluctuations as a function of radius from the field center, averaged in rings. The model fit parameters are given in the figure.

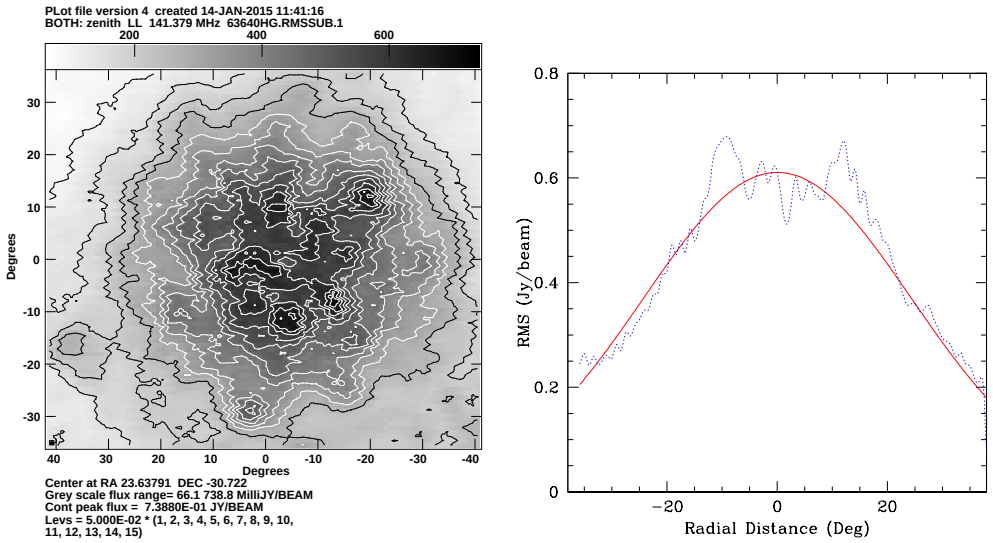

Fig. 9.— Left: The rms fluctuations of surface brightness in Jy/beam across the image, averaged over regions of 24x24 synthesized beams. Right: A cut through the noise distribution in 9a in the North South direction, with a Gaussian fit of FWHM = 57.4^o.

Figure 9a shows the rms fluctuations of surface brightness in Jy/beam across the image, averaged over regions of 24x24 synthesized beams. Figure 9b shows a North-South cut through the peak, with a Gaussian fit. Local peaks are clearly seen. These peaks are due (mostly) to PSF sidelobes from the brightest sources in the field. However, it has been argued that, if bright-source sidelobes could be removed, such a fluctuation-of-fluctuations analysis could have some bearing on large scale clustering of cosmic radio sources.

The FWHM of the Gaussian fit to the primary beam cut in Fig 9b is 57.4^o. This value is significantly larger than the nominal PAPER beam FWHM $\sim 40^o$. Note that I have taken this cut in the North-South direction, hence it should not be adversely affected by the smearing of the noise field due to the 50min averaging. However, there remains the question: in which direction was the dipole oriented? I do note that the Gaussian fit in the East-West direction yielded a similar FWHM.

Figure 8b shows a more detailed analysis of the rms surface brightness distribution as a function of radius, averaged in rings around the field center. I have modeled the distribution along the lines of Condon et al. (2012), including a Gaussian component (corresponding to an approximation of the confusion noise times the Primary Beam), and a constant offset, corresponding to the thermal' noise, or far-out sidelobe noise.

The Gaussian model has a FWHM = 49.4^o, and the confusion noise clearly dominates over most of the field. The confusion noise at the field center has an rms = 1.3 Jy beam^{-1}, at $18'$ resolution and 160MHz.

In Condon et al. (2012), equation 27 gives the expected confusion rms, or some scaled form thereof. However, in a private communication, he suggested using the following equation for our data:

$$\sigma_c = 0.2 \times (\nu_{obs}(\mathrm{GHz}))^{-0.7} \times (\mathrm{FWHM(arcmin)})^2 \text{ mJy beam}^{-1}$$

For the PSA64 parameters, this implies: $\sigma_c \sim 234$ mJy beam^{-1}, which is well below our measurement. However, Jim also says that this equation applies if we can effectively subtract all sources brighter than 5σ prior to calculating the rms. Hence, this calculated value will be a lower limit.

For comparison, the MWA papers quote an (expected) confusion noise $\sim$ 10mJy beam^{-1} to 20mJy beam^{-1} at $\sim 2'$ resolution (Tingay et al. 2013, PASA, 30, 7) at 150MHz. Scaling this to $18'$ with the equation above, leads to $\sim$ 1.2Jy beam^{-1}, more in line with my measurement.